Integrated Transparent Surface Acoustic Wave Technology for Active De-Fogging and Icing Protection on Glass

Hui Ling Ong,[1,#] Deyu Yang,[2,#] Hui Chen,[3] Jian Zhou,[3,*] Luke Haworth,[1] Jikai Zhang,[1], Des Gibson,[4] Prashant Agrawal,[1] Hamdi Torun,[1] Qiang Wu,[1] Xianghui Hou,[2] YongQing Fu,[1,*]

[1] Faculty of Engineering and Environment, Northumbria University, Newcastle upon Tyne, NE1 8ST, UK
[2] State Key Laboratory of Solidification Processing, Shaanxi Key Laboratory of Fiber Reinforced Light Composite Materials, Northwestern Polytechnical University, Xi'an 710072, China
[3] College of Mechanical and Vehicle Engineering, Hunan University, Changsha 410082, China.
[4] Institute of Thin Films, Sensors & Imaging, University of the West of Scotland, Scottish Universities Physics Alliance, Paisley PA1 2BE, UK

#These authors have same contribution to this paper.

*Correponding authors: Dr. Jian Zhou, jianzhou@hnu.edu.cn; Prof. Richard Yongqing Fu, Richard.fu@northumbria.ac.uk

Abstract: There have been great concerns on poor visibility and hazardous issues due to fogging and ice/frost formation on glass surfaces of windshields, windows of vehicles/airplanes, and solar panels. Existing methods for their monitoring and removal include those active ones (such as using resistance heating) or passive ones (such as using surface icephobic treatments), which are not always applicable, effective or reliable. In this study, we proposed a novel strategy by implementing transparent thin film surface acoustic wave (SAW) devices by directly coating ZnO films onto glass substrate and studied their de-fogging, active anti-icing and de-icing mechanisms using the SAW technology. Effects of powers and wavelengths of SAW devices were investigated and influences of acousto-heating and surface hydrophobic treatments were evaluated. Results showed that de-fogging time was dramatically decreased with the increase of SAW powers when the thin film-based SAW devices were exposed to humid air flow for different durations. The icing accretion was significantly delayed under the applied SAW agitation, and SAW application has also effectively promoted de-icing on glass substrate, due to the interfacial nanoscale vibration and localised heating effect.

Keywords: Surface acoustic wave, rime ice, phase change, icing technology

1. Introduction

There are great concerns about fogging, condensation, icing and frosting on glass surfaces, which cause poor visibility and hazard issues in lenses, windshields, windows of vehicles/airplane/helmet, and solar panels [1]–[5]. In conditions with a high humidity in a cold environment, water condensation, icing and frosting can easily occur on the cold structure surfaces, whose surface temperature is at or below the dew point [6], [7], [8]. For instance, foggy conditions can pose safety and hazard issues due to severely decreased visibility which put risks for transportation, and endanger people's health and wellbeing [9], [10]. Moreover, extreme weather conditions frequently result in ice and snow formation on the surfaces of daily items and economically important assets such as the windows and windshields of cars, trains, and airplanes, camera lenses, and traffic lights, resulting in poor operability and safety issues. [1], [4]. Another issue of fogging or icing on glass would be the increased surface roughness on glass during their long term usages, which can cause a negative impact on the mitigation effort [11], [12]. The condensation on glass surfaces will induce unwanted light refraction and result in light scattering, rendering a translucent surface and a reduction in optical transparency [13].

Passive and active methods have been demonstrated to combat surface accretions induced by fogging, icing and/or frosting [14]–[16]. There have been various existing methodologies implemented for the elimination of fogging, and these can be classified into warm fog elimination and cold fog elimination [9], [10], [17]–[19]. Fogging easily occurs at a temperature higher than 0°C called warm fogging, and the techniques to remove this generally require external energy, including external heating, dynamic perturbation method (or mechanical mixing method), or seeding hygroscopic particles [9], [10], [17]–[19]. Cold fogging mainly contains water droplets when the temperature is below 0°C, which usually involves a phase change in the fog (e.g., forming ice crystals in fog) [9], [10]. One common method used for tackling this cold fog is to use refrigerants that can be harmful to the environment [9], [10], [17]–[19]. These methods of eliminating fogging tend to consume a huge amount of energy, and pose as a pollution issue in terms of corrosion [9], [18]. Other methods such as local electrothermal heating are also applied, but their efficiency and power consumption have been major concerns.

Ice formation can be classified into rime ice and glaze (or clear) ice based on their morphologies and densities [20]–[23]. Rapid growth of ice due to supercooled water droplets results in rime ice with features of porous microstructures, low density, high opacity and loose adherence to the structural surface [21], [23]–[25]. Glaze ice, on the other hand, is formed by the freezing of the supercooled liquid water which penetrates the air gaps between the ice particles before it freezes, and this formation usually begins when the temperature is relatively high (e.g., just below the freezing point) [20], [21], [24], [25]. In contrast to rime ice, glaze ice is considerably smooth, compact, more densely packed, transparent, and adhere strongly to the surface [8], [20], [23]. Formation of various types of ice is depending on freezing or condensation

conditions of supercooled liquid droplets on the glass surfaces in an environment with various relative humidity (RH) levels, surface temperatures, and cooling rates [24], [25]. In both cases, they relatively have high ice adhesion to the glass surface, making it tedious to be eliminated from the surface.

One of the key passive anti-icing methods is to reduce surface energy of the solid surface and decrease water-ice adhesion using superhydrophobic and icephobic surfaces [8], [16], [25], [26]. It was reported that the superhydrophobic surfaces with a large contact angle can significantly delay the droplet freezing when compared to those on hydrophilic surfaces [7], [8], [16], [27]. However, these superhydrophobic surfaces often have poor mechanical /adhesion properties and durability issues [28]–[30]. There have been previous studies on various functionally treated surfaces on glass surfaces for ice mitigation [31]–[34], but implementing these surfaces does not often appear to reduce ice adhesion or increase icing protection. Similar to the fogging strategies, active approaches for icing strategies include application of external energy such as heating, mechanical vibrations, liquid chemicals, and ultrasonic waves [14], [23]. However, ice mitigation using these methods often requires large amount of energy or quite complicated to be applied onto substrates such as glass [20]. Hence, it is crucial to search other alternative methods for ice mitigation to achieve highly efficient and environmentally friendly ice protection implementations. If considering icing protection on transparent and often fragile glass surfaces, most of these active methods would have a huge challenge to cope with.

Recently, an emerging technology for fog/ice mitigation is to incorporate coating or thin film-based surface acoustic wave (SAW) devices directly onto the component structures to produce acoustic wave propagation and vibrations directly integrated onto the structural surfaces, such as glass or metals, which can be integrated for fogging, anti-icing and de-icing functions [35]–[37]. SAWs have been widely employed in various applications such as wireless communications, acoustofluidics, sensing, and particle/biological manipulations [35], [38]–[40]. Multiple wave modes (which include Rayleigh, Lamb, Love, and shear horizontal waves) and their harmonic modes of the fundamental waves can be produced and travel along the surface of the SAW devices [35], [36]. These thin film SAW devices can generate strong interfacial vibrations and effective local heating effects [35], [41], [42].

As illustrated in Figure 1, at the localised area where the fog or ice is being accumulated, SAWs can cause effective nanoscale vibration and acousto-thermal effects, which allow fog/ice interface to break, local melting, and ice separation from substrate [36], [43], [44]. Therefore, using SAW technology along with surface hydrophobic treatments, it is possible to combat surface accretions and fog/ice formation [36], [45], [46]. Although there are previous reports for the development of transparent thin film SAW devices for optical, sensing, or wearable device applications [47]–[50], there are few studies using thin film SAWs directly integrated onto glass (see Figure 1) as a transparent platform for fogging or ice mitigation strategies [29], [51]. The great challenge is how to integrate acoustic wave devices onto the transparent glass

with good icing efficiency, while without causing major issues of influences on its transparency and functionality. Figures S1(a) and S1(b) in the supporting information presented the illustrations of the structural design and side-view structural design of the thin film SAWs on glass with respect to the covering area for fogging, freezing droplet and rime ice.

In this paper, we proposed a novel strategy by implementing transparent ZnO thin film SAW devices directly onto glass substrate. For this integrated SAW icing device structure illustrated in Figure 1, the IDTs, piezoelectric film, and glass could be all transparent in principle. Another potential advantage (although we have not realised in this study) is that the piezoelectric thin film will only need to be deposited onto the IDT region to generate waves, and once the SAWs are generated, they will propagate along the glass surfaces without need of piezoelectric films on the other glass areas [36]. In this study, we fabricated SAW devices on glass substrates with different wavelengths and studied their de-fogging and active anti-icing and de-icing mechanisms using SAW technology. Effects of SAW powers, frequency, acousto-heating, and surface treatments with a hydrophobic layer were evaluated. Results showed that de-fogging time was dramatically decreased with the increase of SAW powers. With the introduction of a hydrophobic polymer layer on the SAW surface, the icing accretion was significantly delayed under SAW agitation, and SAW application has effectively promoted de-icing, due to the interfacial nanoscale vibration and local heating effect.

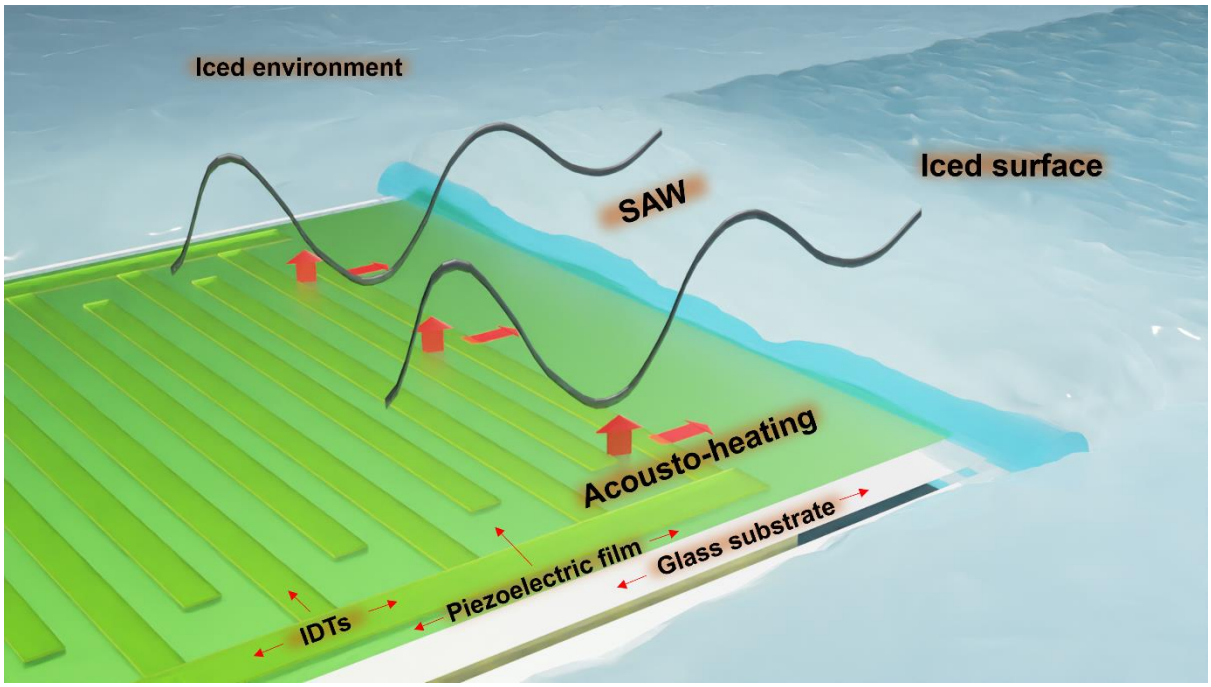

Figure 1. Illustration of structural design of thin film-based SAW device integrated onto the glass substrate

2. Experimental details

2.1.Preparation and characterization of SAW device

ZnO thin film of ~4.5 µm thick was deposited on four-inch borosilicate glass wafer using a direct current (DC) magnetron sputter (NS3750, Nordiko) with a zinc target (99.99% purity). Before the deposition, the glass substrates were cleaned using acetone, isopropanol (IPA), and then deionized (DI) water, finally dried using nitrogen gas. The distance between the glass substrates and ZnO target was 20 cm. The vacuum pressure of the sputter chamber was maintained at ~0.35 Pa. During the deposition process, the surface of the Zn target was oxidized and sputtered by introducing the flows of the argon and oxygen gases with an Ar/O_2 flow ratio of 10/15 SCCM (standard cubic centimetre per minute). The plasma power was set at 400 W. Cross-section morphology of the ZnO film on glass surface was observed using a scanning electron microscope (Tescan Mira). Crystalline structure of the ZnO film was analysed using an X-ray diffractometer (XRD, D5000, Siemens, Cu-Kα radiation, 40 kV, 30 mA).

To fabricate SAW devices, interdigital transducers (IDTs) were patterned on top of ZnO/glass thorough a conventional photolithography and lift-off process. For simplicity, a bilayer of Cr/Au with thicknesses of 20 nm/100 nm was prepared as the electrode in this study. For future applications, this electrode can be prepared using sputtered transparent indium tin oxide (ITO) or aluminium doped ZnO (AZO) for optical transparency [47], [52]. The designed IDTs had 30 pairs of fingers with three different wavelengths (i.e., 100 µm, 200 µm, and 300 µm). The reflection spectra (S11) and transmission spectra (S12) of the SAW devices were measured using an RF network analyser (Keysight, FieldFox N9913A).

2.2. Fogging and icing tests

To evaluate effects of surface treatments on fogging and icing studies, the ZnO/glass SAW device's surfaces were uniformly coated with a layer of fluoropolymer, CYTOP (CTL809 M, Asahi Glass Co.) to create a hydrophobic layer [53]. The choice of CYTOP over other hydrophobic coatings is due to its transparency and a low coefficient of optical dispersion. Additionally, CYTOP can easily be coated on any solid surface and help to reduce ice adhesion on roughened surfaces [54]. For the experiments, the CYTOP layer was deposited in front of the IDTs towards the direction of the propagating waves. The process of surface treatment involved the deposition of a thin layer of CYTOP onto the pre-cleaned surface of the ZnO/glass SAW device via a dip coating method to ensure a uniform coating across the entire SAW device. The sample was then placed inside the tube furnace at 150 °C for 25 minutes for the curing process, and the obtained surface of the ZnO/glass SAW device was covalently bonded with the fluoropolymer chains. The thickness of the CYTOP layer was approximately 10 nm [54]. The water contact angle (WCA) was measured at room temperature using a drop shape analyser (KRUSS Scientific, DSA-30). For creating SAWs, an RF signal at the resonant frequency of

the SAW device was generated using a signal generator (Aim TTi, TG5011A) and was further amplified using a power amplifier (Amplifier Research, Model 75A250). The RF powers applied to the IDTs of the ZnO/glass SAW devices was measured using an RF power meter (Racal Instruments 9104).

De-fogging tests were performed using the ZnO/glass SAW devices, which were placed in the centre of a cold chamber with its substrate pre-set at three different temperatures, i.e., room temperature, ~5°C, and ~0°C. To effectively generate condensation on the surface of the ZnO/glass SAW device, a nebuliser was used, and the relative humidity (RH) was set to be 100%. When the temperature of the ZnO/glass SAW device reached the set value, cold humid air was blown into the side of chamber through a long tube continuously for either 1 minute or 10 minutes. After exposure to the humid air, condensation was seen to form on the surface of the ZnO/glass. Various RF powers (ranged from 0.63 W to 3.41 W) were applied to the SAW devices to remove the moisture and the total time taken for the fogging disappearance was recorded.

For the active anti-icing tests of deionised droplets, a single water droplet with a size of 6.5 µL was deposited onto the glass surface, right in front of the IDT area to form a glaze ice droplet. The tests were performed using the drop shape analyser (KRUSS Scientific, DSA-25) with a cold chamber. The temperature was set to be approximately -20 °C during the tests. The active anti-icing experiments were performed using different SAW powers (from 0.21 W to 0.81 W) applied to the ZnO/glass device.

For de-icing of rime ice on glass substrate, the experiments were conducted in a freezing chamber which was maintained at a stable and constant icing/anti-icing environment, as reported in Ref. [37]. Different relative humidity (RH) levels were achieved using a moisture nebuliser (Omron Ultrasonic Nebulizer NE-U17) that generated water aerosols with controlled vaporizing power and imputing speed. The SAW device was put on a cold plate which was set at -6.5 ℃ and the environmental chamber's average temperature was -1 ℃. Before the start of icing, the SAW device was cooled down in the chamber for at least 30 minutes in advance. Then the icing process was carried out with a RH value of 90%. The de-icing tests were performed using different SAW powers (from 0.002 W to 2.35 W) applied to the ZnO/glass device. The video camera (IDS) with a Navitar 12X objective lens was used to record the changes of ice morphology from the top and side views of the glass device.

For evaluation of the induced surface heating effects during the fogging and icing processes upon SAW agitations, an infrared (IR) camera (FLIR, T620bx) was used to monitor the temperature changes on the SAW device surface at different RF powers. This temperature measurement was taken in front of the IDTs area, where the droplets and condensates were located for the icing and fogging tests.

3. Results and discussions

3.1.Characterisation of ZnO thin films and SAW devices

Figure 2(a) shows the XRD spectrum of the ZnO thin film on glass. A strong peak at 34.1º corresponds to the (0002) plane of ZnO film, which shows the c-axis preferential growth of the Wurtzite ZnO film. Figures 2(b) shows an SEM image of cross-section image of ZnO film on glass substrate, which shows the vertical columnar structure with a film thickness of ~4.5 microns. Once the RF power is applied to the SAW devices, there is an acousto-thermal effect generated and thus the surface temperature has been increased. For verifying this acoustic heating effect, we have measured the surface temperatures obtained from IR camera readings approximately 5 mm from the front of the IDTs at different applied powers for the SAW devices with the frequency of 28 MHz. The results are shown in Figure 2(c). The surface temperature increases rapidly in the initial 30 seconds during SAW agitations. For example, as the applied power increased from 1.41 W to 7.59 W, the temperature at position of 5 mm right in front of the IDTs was observed to increase to ~98ºC. The inset image in Figure 2c shows an example of the infrared images, revealing the thermal distribution on the surface of the ZnO/glass SAW device. The detailed information and mechanisms on thermal effects for the thin film SAW devices was reported in our previous studies [14], [55], [56]. Figure 2(d) shows the temperature readings obtained from IR camera for 9 MHz SAW device at different applied RF powers. Similar to those shown in Figure 1(c), the surface temperature increases steadily during the heating process, and the maximum temperature is changed from 18°C to 28°C with the applied power varied from 0.052 W to 21.8 W. In comparison between the two frequencies of SAW devices, 28 MHz SAW device shows a higher acousto-heating effect than that of 9 MHz SAW device.

The water contact angle (WCA) of droplets with and without any surface treatments on the glass surface were measured. Without any surface treatment, the ZnO/glass SAW device was observed to have a WCA of 88.2±0.6º. With the addition of CYTOP layer onto ZnO/glass SAW device, the WCA was increased to 106.4±0.8º. The quality factors (Q-factor) of the SAW devices were estimated from the reflection spectrum S11 peak and the average reading is 68.7.

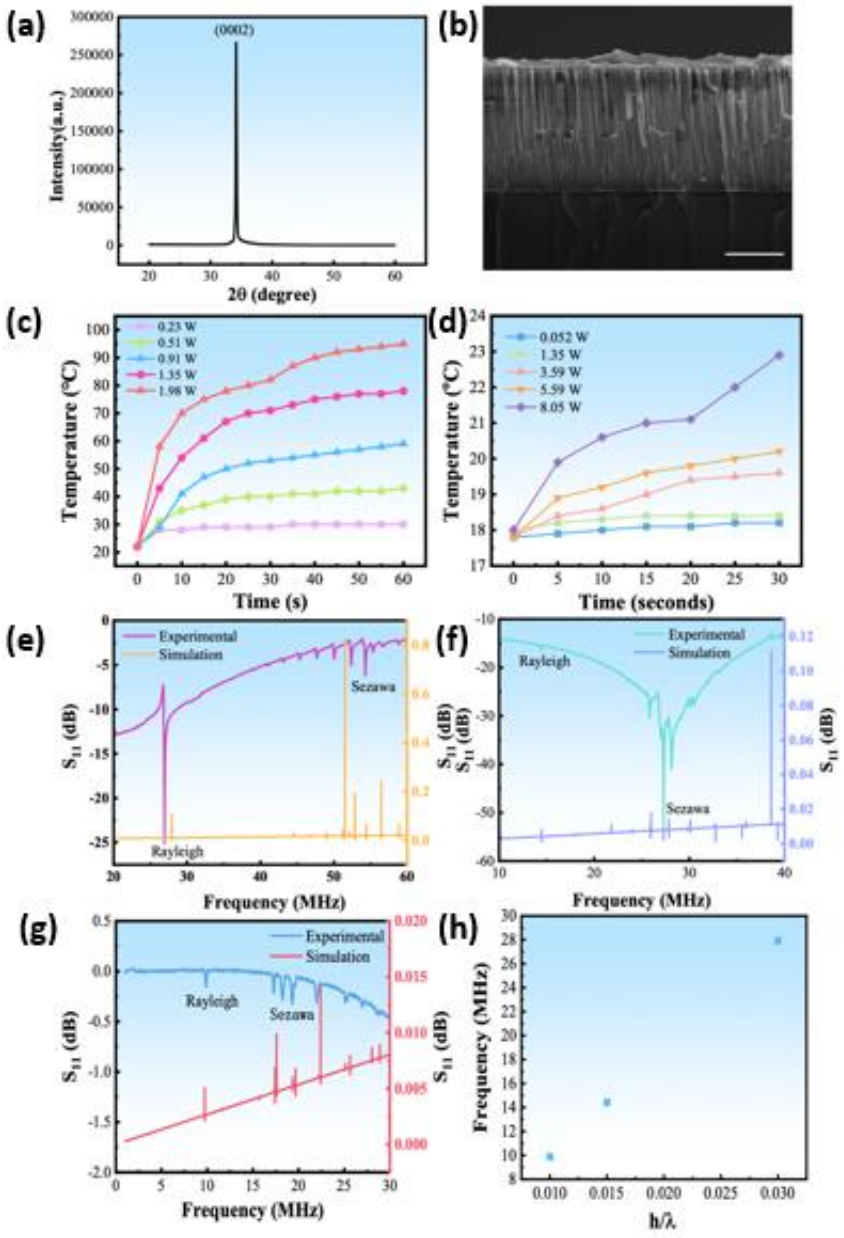

Figure 2: (a) XRD pattern of ZnO/glass SAW device; (b) SEM image showing the cross section of ZnO film; (c) Temperature changes of the 28 MHz SAW device as a function of SAW power and time; (d) Temperature changes of the 9 MHz SAW device as a function of SAW power and time; Frequency responses (S11) of ZnO/glass SAW devices with wavelengths of (e) 100 µm; (f) 200 µm; (g) 300 µm; (h) Frequencies as a function of normalised thickness.

Numerical simulations were performed using finite element analysis (FEA) with the commercial software (COMSOL 5.1) based on a two-dimensional (2D) strain model of a piezo plane to investigate the surface vibration patterns and wave modes of the ZnO/glass SAW devices with different wavelengths. For simplification of simulations, we modelled a 5 µm

thick ZnO layer on a 120 μm thick glass layer with a fixed boundary condition at the bottom. We have verified that this glass thickness was thick enough to allow for acoustic wave penetrations into the glass substrate without influencing the simulation outcomes. A layer of 200 nm thick aluminium electrode received a 1V polarisation voltage, and the second electrode was served as electrical ground. The COMSOL material library was used to obtain the material constants. The devices' wavelength was changed from 100 to 300 μm.

Figures 2(e) to 2(g) show the simulated results of impedance spectra, and also the experimentally obtained reflection spectra (S11) of the ZnO/glass SAW devices with different wavelengths of 100 μm, 200 μm, and 300 μm. Based on the simulated vibration modes, the resonant frequencies of the Rayleigh waves were identified at 28.01 MHz, 14.43 MHz, and 9.81 MHz, respectively, which are similar to those of the experimentally obtained data of 27.92 MHz, 14.42 MHz, and 9.88 MHz. The Sezawa modes were also identified from the vibration patterns, and they are at frequencies of 51.53 MHz, 28.19 MHz, and 19.02 MHz, while the experimentally obtained values are 51.84 MHz, 28.84 MHz, and 19.76 MHz, for three different devices, respectively. In this study, we applied these Rayleigh wave modes for fogging and icing experiments. Figure 2(h) shows the frequencies of the SAW devices increases with the normalized thickness. This is mainly due to propagation of the acoustic wave confining in the piezoelectric ZnO layer with the higher frequencies [53]. Figures S2(a) to S2(f) in the supporting information show the obtained particulate vibration profiles of both Rayleigh and Sezawa modes for the three different wavelengths (i.e., 100 μm, 200 μm, and 300 μm) from the simulation results, which are verified from the simulated impedance of those devices.

3.2. De-fogging performance

Figures 3(a) to 3(d) show the averaged times taken for removal of the generated condensation on the device surfaces, which were pre-exposed to the humid air flowing after the durations of 1 minutes and 10 minutes, respectively, for both 9 MHz and 28 MHz SAW devices. The time taken for fog elimination was calculated based on the duration in which SAW agitations prompted the driving action which occurred near the IDT area of the SAW device. Results show that the time taken to achieve de-fogging is dramatically decreased with the increase of SAW powers as expected for both the cases. It was noted that with CYTOP on the 9 MHz ZnO/glass SAW device, the time taken to achieve de-fogging is also reduced as compared to the untreated ZnO/glass SAW device. Also, the time taken for the case to remove the de-fogging when exposure to humid air for 10 minutes is much longer than that for 1 minute, mainly due to significant increased amounts of condensation on the sample surface. In terms of temperature effects, a much shorter time was recorded to remove the condensates using the SAW device for the surface tested at room temperature. As more condensates were formed at near 0 °C as compared those at near 5 °C and at room temperature, a much longer time was needed. After the SAW RF power is applied onto the SAW device, the mechanical vibrations

from SAW agitations induces internal acoustic streaming in the condensates, and a strong localized acousto-thermal effect is also generated [37], [57]. As the waves propagate on the surface, they drive away the condensates or evaporate them effectively, thus achieving the de-fogging effect. There are dramatic reductions in the de-fogging time as shown in Figure 3 where the CYTOP is shown to prompt the de-fogging process more effectively than that of untreated ZnO/glass SAW devices. Comparing the time taken for the two devices with different frequencies, a much shorter time was found for the 9 MHz SAW device, which can be explained due to its higher amplitude of vibration pattern and larger wavelength.

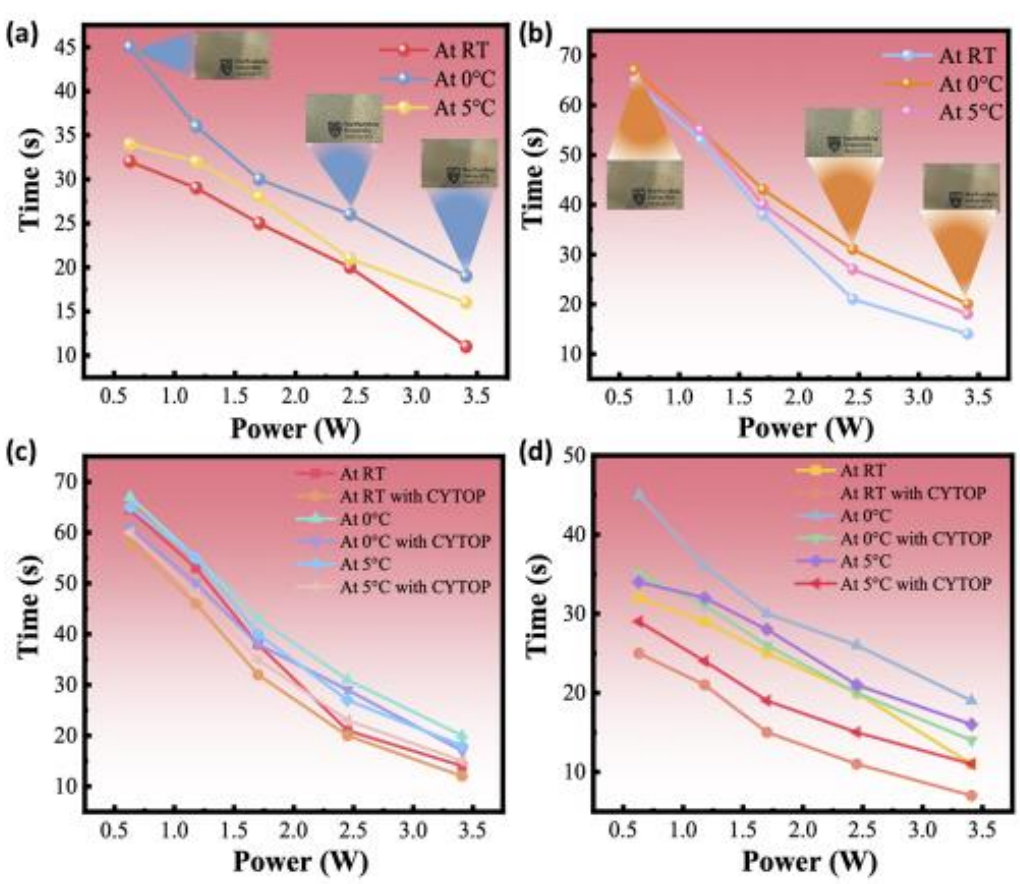

Figure 3: Illustrations of the de-fogging process for 28 MHz ZnO/glass SAW device; (a) 1 minute exposure to humid air; (b) 10 minutes exposure to humid air; De-fogging process for 9 MHz ZnO/glass SAW device (c) 1 minute exposure to humid air; (d) 10 minutes exposure to humid air

3.3.Active Anti-icing performance

Droplet freezing was first conducted on untreated ZnO/glass SAW device, without using SAW energy. The captured shape evolutions of the droplet during glaze icing are shown in Figure 4(a), where icing is shown to occur after ~19 seconds. The snapshots at different time frames depict that the freezing front tip moves upwards and the remaining part of water droplet which

was not frozen remains a spherical shape [58]–[60]. At a time of ~80.9 s, the ice expands vertically and pushes against the spherical cap of the liquid water droplet. With the addition of confining effect of surface tension, it leads to the pointy tip as seen at ~91.4 s [58], [59].

Droplet freezing was then conducted at RH 45% on ZnO/glass SAW device which was surface treated with CYTOP but without applying any SAW power, and the obtained results are shown in Fig. 4(b). At the same testing conditions, glaze icing was observed to start to form at ~42.3 seconds, with the frozen phenomena like those of untreated ZnO/glass SAW device, and ice crystal was formed after ~109 seconds. It was observed that with the implementation of hydrophobically treated CYTOP layer, the droplet freezing was delayed compared with the untreated samples.

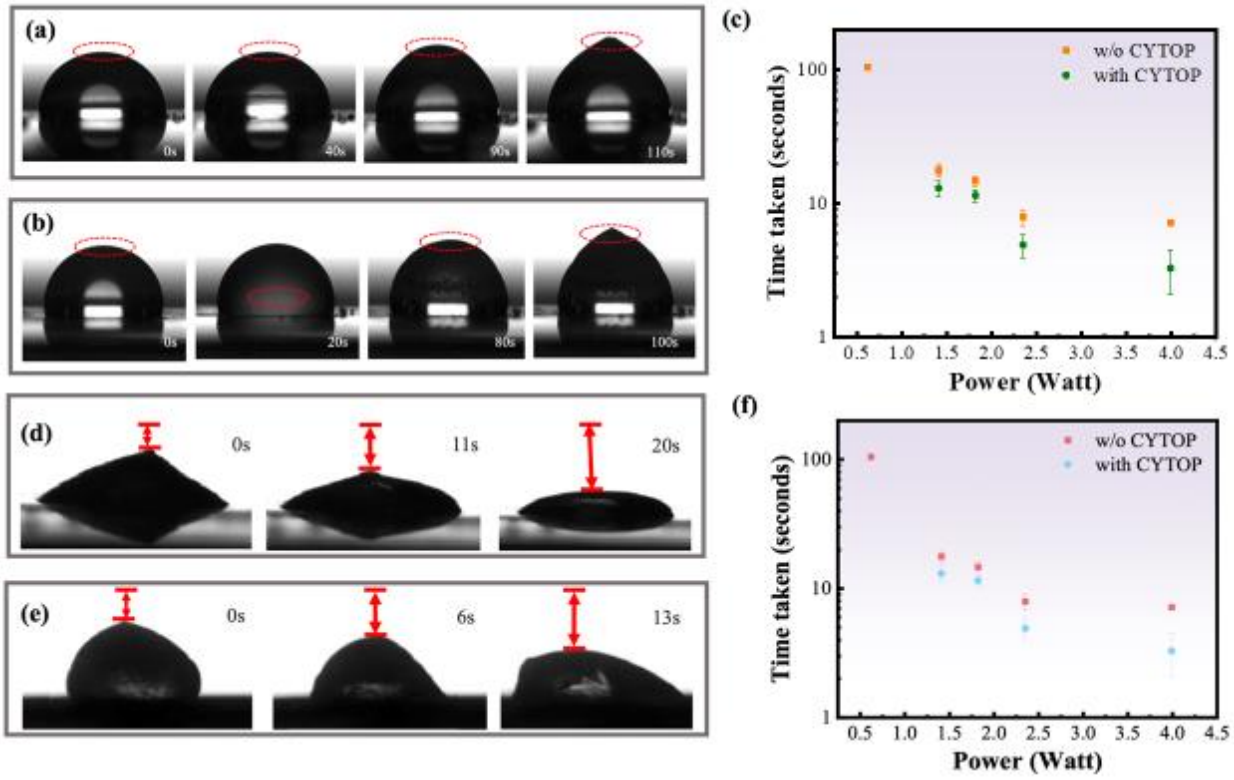

Figure 4: Droplet freezing on ZnO/glass SAW device at RH 45% (a) untreated surfaces, (b) CYTOP treated surfaces; (c) Time taken for droplet to become ice on ZnO/glass SAW device at various RF powers; De-icing on ZnO/glass SAW device (d) without CYTOP at 1.41 W; (e) with CYTOP treatment at a power of 1.41 W; (f) Time taken for droplet de-icing at various RF powers.

Figure 4(c) shows the time taken for droplet to become ice with and without SAW agitations at different RF powers. Without applying any RF power (e.g., at zero Watts), the time taken for the water to become ice for both treated and untreated surfaces possessed similar readings. Under SAW agitations at a much lower power, such as 0.21 W, the induced insignificant

surface vibrations prevent the possibility for the formation of supercool liquid droplets. Therefore, the ice formation time was slightly decreased compared with those without applying any waves, mainly due to significant surface vibrations and prevent formation of supercooled liquid and increases the chances for the formation of ice nucleolus on the device's surface [37] [42]. The heating effect at such a low power was not strong enough to prevent the ice nucleus formation. However, when SAW powers were increased to 0.37 W and above, the delayed frozen time has been gradually increased and becomes significantly longer at higher powers, showing good active anti-icing effects. When the RF power was increased further to 0.62 W and 0.81 W, no frozen phenomena of the droplet was observed at all after 600 seconds (the maximum time we have applied before stopping).

When large amplitude SAWs (i.e., at a high SAW powers) are generated and propagate along the surface of ZnO/glass SAW device, the nanoscale 'earthquake' effect, along with acoustic radiation force and acoustic streaming will hinder the ice nucleation and growth [37], [46]. When there are ice nuclei formed within the liquid, they will be driven by acoustic streaming, and this results in the relative motion of the ice nucleolus and liquid medium upon SAW agitation into the liquid [37], [46]. This flow is enhanced upon increasing application of RF powers and the formed ice nucleoli are easily detachable from the surface into the liquid. Additionally, the localized thermal effect along with the SAWs at interface of the ice/structure causes the increase in temperatures of the glass surface and the surrounding liquid [37], [46].

3.4.De-icing performance under SAWs

Figures 4(d) show the de-icing results for glaze ice using the ZnO/glass SAW devices at a power of 1.41 W. On the untreated device surface, there were changes in the ice shapes when the SAW was applied, which can be due to the introduction of strong localized vibrations and acousto-thermal effect at the ice/glass interface due to the SAWs [37]. During the deicing process, tiny cracks could be generated at the solid/ice interfaces and the growth of these cracks were increased with the continuous SAW agitations, which has also been previously reported in Ref. [37]. Due to the formation and propagation of cracks, the mechanical adhesion of ice to the glass surface is weakened. Simultaneously due to the localized acousto-heating effects, the ice at the interfaces also starts to become partially melted as shown in Figure 4(f), before it is changed further into liquid [37].

Figures 4(e) shows the shape evolution of clear ice with CYTOP when the SAW power was applied, and the obtained phenomena are similar to those illustrated in Figures 4(d). With applying the layer of CYTOP in Figure 4(e), the time taken to de-ice was reduced. This further suggests that surface treatment with CYTOP helps to promote the de-icing performance. Figure 4(f) summarizes the time taken for the droplet to achieve the de-icing. It was observed that the time taken for the de-icing was reduced as the RF powers were increased.

We further studied the deicing for the rime ice formed on the SAW devices. Figures S3(a) to S3(d) in the supporting information illustrate the changes of transparency of ZnO/glass SAW devices during rime ice formation and after deicing process, where the assessment of transparency is based on the film coated glass areas without the IDTs. It was observed that the transparency of ZnO/glass SAW device was decreased at different cooling stages due to the ice formation where a university logo for Northumbria University was hardly visible. After deicing using SAWs, the glass became clear again as the rime ice was removed.

Figures 5(a) to 5(f) illustrates top-view de-icing process of the rime ice on 28 MHz ZnO/glass SAW device which was treated with CYTOP. The morphology of the rime ice was observed to be solid, porous and loosely attached to the surface as shown in Figure 5(a). When RF powers are applied, the mechanical vibrations from the SAW acoustic energy damage the interface of the rime ice clusters with substrate, which leads to the change in the microstructures of the porous rime ice and its morphology as shown in Figure 5(b). During the experiments rime ice has been removed from particular areas. Due to the significant vibrations at the interface, additional new areas of rime ice removal are generated as depicted in Figure 5(c). Other than the mechanical vibrations from the applied RF power, interficial localised heating (acoustic thermal effect) is also induced on the ZnO thin film due to SAW energy dissipation [37], and this can be observed in Figure 5(d). This will eventually lead to the shrinkage and removal of the porous rime ice as observed in Figure 5(e). As time progresses, multiple porous rime ice will continue to shrink and be removed, which fulfills the de-icing process as a result from SAW agitations and acousto-thermal effect as depicted in Figure 5(f).

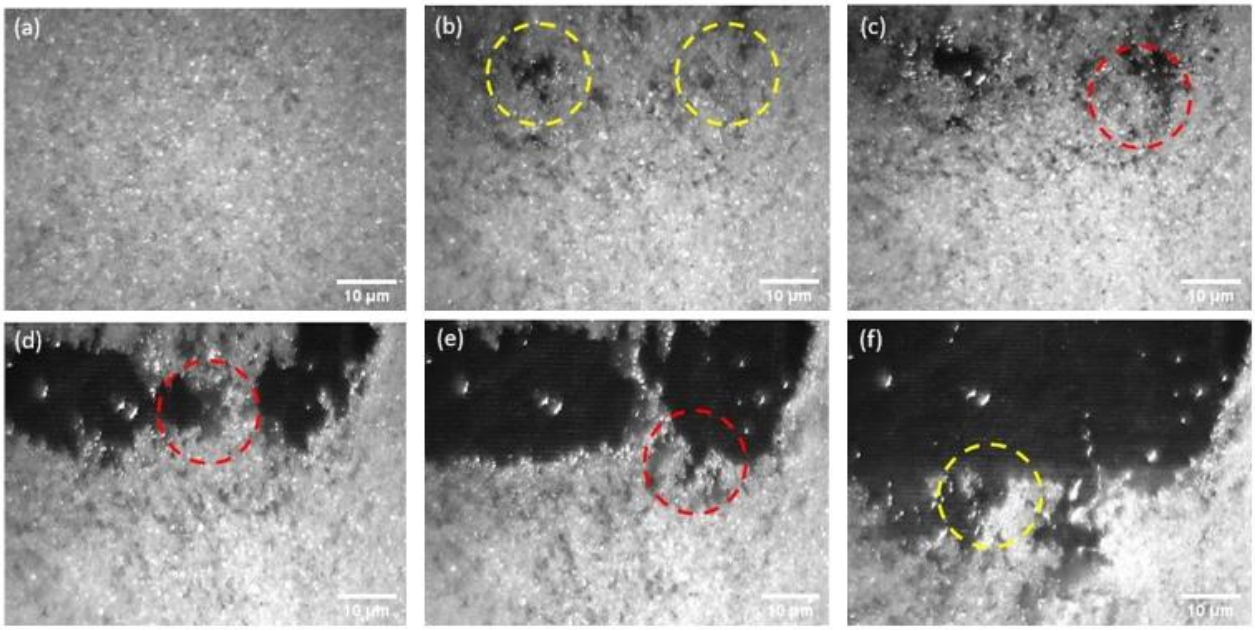

Figure 5: Rime ice de-icing process of ZnO/glass SAW device with a scale bar of 10 µm: (a) 0 s, (b) 5.912 s, (c) 6.868 s, (d) 8.420 s, (e) 10.988 s, (f) 34.040 s

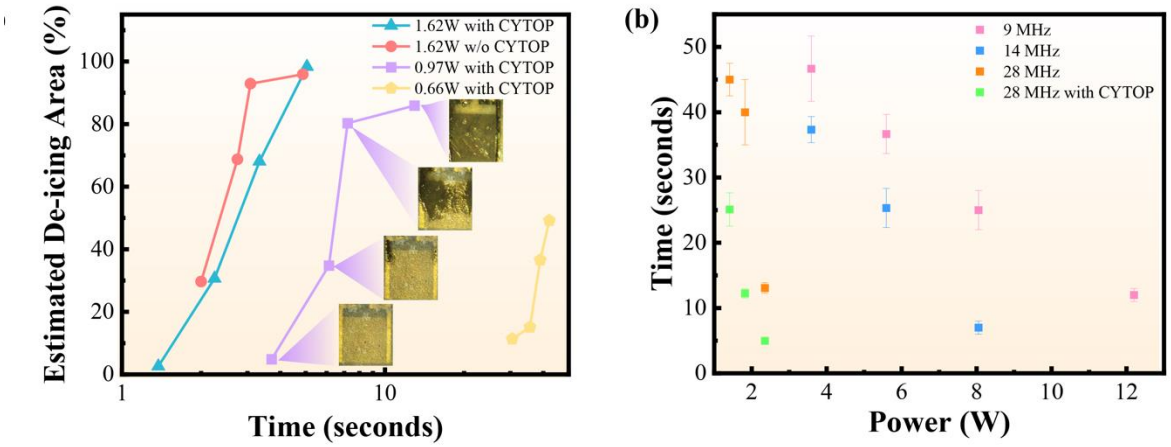

Figure 6: (a) Estimated de-icing areas (%) versus time (seconds) for ZnO/glass SAW device at different powers with and without CYTOP treatment. The inset images show the surface morphologies of SAW devices treated with CYTOP at 0s, 2.250s, 4.333s, and 5.052s; (b) De-icing time of rime ice at different frequencies (9 MHz, 14 MHz, and 28 MHz) and with CYTOP treatment for 28 MHz

Figure 6(a) shows estimated de-icing areas (i.e., the percentages of areas with their ice removed compared with the originally total area) for the ZnO/glass SAW device at different RF powers. With the increase of SAW powers, the de-icing efficiency has been improved dramatically (i.e., the deicing areas have increased signficantly). Figure 6(b) summarises the time taken for rime ice de-icing at different frequencies (i.e., 9.88 MHz, 14.42 MHz, and 28.01 MHz) and for both untreated and treated samples (i.e., 28.01 MHz). It was observed that de-icing is much more efficient for higher frequency samples as shorter time was required to remove the rime ice on the surface within a given area. Compared with those of lower frequency samples, the increase in frequency (or decrease in wavelength) causes the SAW acoustic energy to be easier absorbed or dissipated into the rime ice and also the melting of liquid as de-icing process occurs, resulting in higher rate of energy dissipation [61], [62]. This would further suggest that for de-icing processes, acousto-thermal effect has its contribution for deicing, where the temperature increases rapidly on a localised area, and this can be supported by the IR camera results presented in Figure 2(d) and 2(e). However, we should address that with the increase of the frequency (or decrease of wavelength), the SAW agitated areas become much smaller, mainly due to the faster dissipation of wave energy.

With CYTOP treatment, the time taken for removing the ice is relatively shorter and this suggests that the hybrid effect of combining passive CYTOP coating and active SAW agitation is effective for ice mitigation. The reduced ice adhesion and surface energy after hydrophobic treatment enhances the separation of ice/structure interfaces and also increases the mobility of surface melted liquid which accelerates the ice removal. As explained before, during the icing process, tiny cracks are usually created at the ice-structure interface and the nanoscale vibrations induced by SAWs enhance the rapid growth of these cracks [37], [46], and acousto-thermal effect induced localized melting of the interfacial ice layer, both of which reduce the ice adhesion force [37], [46].

4. Conclusions

Transparent ZnO thin film SAW device was made and then applied for realising de-fogging, active anti-icing and de-icing functions on glass surfaces. Different RF powers were applied to evaluate the efficiency of both antifoggin and icing issues. De-fogging time was dramatically decreased with the increase of SAW powers when the SAW devices were exposed to humid air flow. When the SAW is applied at different RF powers, formation of the ice has been signficantly delayed and both clear ice and rime ice formed on the SAW devices have been effectively removed, due to strong localised vibrations and acousto-thermal effect at the ice/glass interface during SAW operation. Additionally, the introduction of CYTOP on SAW surface has an effect on the time taken for active anti-icing and de-icing at different RF powers, which further prompted that the hybrid ice mitigation with the CYTOP treatment.

Acknowledgement

This work was supported by the Engineering and Physical Sciences Research Council of UK (EPSRC EP/P018998/1), UK Fluids Network Special Interest Group of Acoustofluidics (EP/N032861/1), EPSRC Centre for Doctoral Training in Renewable Energy Northeast Universities (ReNU) for funding through grant EP/S023836/1, and International Exchange Grant (IEC/NSFC/201078) through Royal Society and the Natural Science Foundation of China (NSFC).

References

[1] K. Kasahara, T. Waku, P. W. Wilson, T. Tonooka, and Y. Hagiwara, “The Inhibition of Icing and Frosting on Glass Surfaces by the Coating of Polyethylene Glycol and Polypeptide Mimicking Antifreeze Protein,” *Biomolecules*, vol. 10, no. 2, Feb. 2020,

doi: 10.3390/BIOM10020259.

[2] L. Tian, Z. Zhang, X. Jiang, L. Shu, J. Hu, and H. Qin, “Study on the Icing Accretion Characterization of Porcelain and Glass Insulator,” *ICHVE 2018 - 2018 IEEE Int. Conf. High Volt. Eng. Appl.*, Feb. 2019, doi: 10.1109/ICHVE.2018.8642201.

[3] X. Du, Z. Yang, Z. Jin, Y. Zhu, and Z. Zhou, “A numerical prediction and potential control of typical icing process on automobile windshield under nocturnal radiative cooling and subfreezing conditions:,” *https://doi.org/10.1177/0954407019875356*, vol. 234, no. 5, pp. 1480–1496, Sep. 2019, doi: 10.1177/0954407019875356.

[4] A. Ene and C. Teodosiu, “Studies dealing with defogging and de-icing phenomena on vehicles’ windshield: A review,” *IOP Conf. Ser. Earth Environ. Sci.*, vol. 664, no. 1, May 2021, doi: 10.1088/1755-1315/664/1/012071.

[5] I. R. Durán, J. Profili, L. Stafford, and G. Laroche, “Unveiling the origin of the anti-fogging performance of plasma-coated glass: Role of the structure and the chemistry of siloxane precursors,” *Prog. Org. Coatings*, vol. 141, p. 105401, Apr. 2020, doi: 10.1016/J.PORGCOAT.2019.105401.

[6] J. Carroll, “Water content of natural gas,” *Nat. Gas Hydrates*, pp. 307–345, Jan. 2020, doi: 10.1016/B978-0-12-821771-9.00010-0.

[7] Z. Zhang, S. Lv, S. Mehendale, L. Yan, H. Yuan, and J. Tian, “Visual study of the freezing process of a water droplet on a horizontal copper plate,” *Authorea*, vol. 1, pp. 1–36, 2020, doi: 10.22541/au.160316286.66554116/v1.

[8] K. Xu, J. Hu, L. Shu, X. Jiang, and Z. Huang, “Influence of hydrophobicity on ice accumulation process under sleet and wind conditions,” *AIP Adv.*, vol. 8, p. 35113, 2018, doi: 10.1063/1.5022422.

[9] C. Liu, Z. Tian, Y. Zhao, and X. Zeng, “Review and prospect of fog elimination technology based on acoustic condensation,” *IOP Conf. Ser. Earth Environ. Sci.*, vol. 514, no. 3, Jul. 2020, doi: 10.1088/1755-1315/514/3/032011.

[10] C. Liu, Y. Zhao, Z. Tian, and H. Zhou, “Numerical Simulation of Condensation of Natural Fog Aerosol under Acoustic Wave Action,” *Aerosol Air Qual. Res.*, vol. 21, 2003, doi: 10.4209/aaqr.2020.06.0361.

[11] P. O. A. Borrebæk, S. Rønneberg, B. P. Jelle, A. Klein-Paste, Z. Zhang, and J. He, “A framework for classification of snow- and icephobicity,” *J. Adhes. Sci. Technol.*, vol. 35, no. 10, pp. 1087–1098, 2021, doi: 10.1080/01694243.2020.1834286.

[12] P. O. A. Borrebæk, B. P. Jelle, and Z. Zhang, “Avoiding snow and ice accretion on building integrated photovoltaics – challenges, strategies, and opportunities,” *Sol. Energy Mater. Sol. Cells*, vol. 206, Mar. 2020, doi: 10.1016/J.SOLMAT.2019.110306.

[13] W. Li *et al.*, “Transparent selective photothermal coatings for antifogging applications,” *Cell Reports Phys. Sci.*, vol. 2, no. 5, p. 100435, May 2021, doi: 10.1016/J.XCRP.2021.100435.

[14] M. Yamazaki, A. Jemcov, and H. Sakaue, “A review on the current status of icing physics and mitigation in aviation,” *Aerospace*, vol. 8, no. 7, 2021, doi: 10.3390/aerospace8070188.

[15] M. A. S. Shohag, E. C. Hammel, D. O. Olawale, and O. I. Okoli, “Damage mitigation

techniques in wind turbine blades: A review," *Wind Eng.*, vol. 41, no. 3, pp. 185–210, Jun. 2017, doi: 10.1177/0309524X17706862.

[16] N. Dalili, A. Edrisy, and R. Carriveau, "A review of surface engineering issues critical to wind turbine performance," *Renew. Sustain. Energy Rev.*, vol. 13, no. 2, pp. 428–438, Feb. 2009, doi: 10.1016/J.RSER.2007.11.009.

[17] Y. H. Jia, F. F. Li, K. Fang, G. Q. Wang, and J. Qiu, "Interaction between strong sound waves and cloud droplets: Theoretical analysis," *J. Appl. Meteorol. Climatol.*, vol. 60, no. 10, pp. 1373–1386, 2021, doi: 10.1175/JAMC-D-20-0278.1.

[18] M. Zhang *et al.*, "Experimental study on coalescence of fog droplets in cloud chamber under low-frequency sound waves," *JPhD*, vol. 54, no. 39, p. 395301, Sep. 2021, doi: 10.1088/1361-6463/AC100A.

[19] H. Czyż, T. Markowski, and H. Czy, "ACOUSTIC METHOD OF AIRPORT FOG PRECIPITATION," *Aviation*, vol. XI, pp. 26–30, 2007, doi: 10.1080/16487788.2007.9635966.

[20] H. Dai, C. Zhu, H. Zhao, and S. Liu, "A new ice accretion model for aircraft icing based on phase-field method," *Appl. Sci.*, vol. 11, no. 12, 2021, doi: 10.3390/app11125693.

[21] G. Fortin, J. L. Laforte, and A. Ilinca, "Heat and mass transfer during ice accretion on aircraft wings with an improved roughness model," *Int. J. Therm. Sci.*, vol. 45, no. 6, pp. 595–606, Jun. 2006, doi: 10.1016/J.IJTHERMALSCI.2005.07.006.

[22] Y. Yin, L. Cheng, W. Wang, Y. Zhang, and Y. Liang, "Rime ice growth characterized by surface acoustic wave ARTICLES YOU MAY BE INTERESTED IN SAW-driven droplet jetting technology in microfluidic: A review Biomicrofluidics," *AIP Adv.*, vol. 11, p. 115028, 2021, doi: 10.1063/5.0069716.

[23] Y. Liu, L. J. Bond, and H. Hu, "Ultrasonic-attenuation-based technique for ice characterization pertinent to aircraft icing phenomena," *AIAA J.*, vol. 55, no. 5, pp. 1602–1609, 2017, doi: 10.2514/1.J055500.

[24] Y. Liu, W. L. Chen, L. J. Bond, and H. Hu, "Development of an ultrasonic pulse-echo (UPE) technique for aircraft icing studies," *AIP Conf. Proc.*, vol. 1581 33, pp. 1757–1764, 2014, doi: 10.1063/1.4865036.

[25] F. Tarpoudi Baheri, L. D. Poulikakos, D. Poulikakos, and T. M. Schutzius, "Dropwise condensation freezing and frosting on bituminous surfaces at subzero temperatures," *Constr. Build. Mater.*, vol. 298, p. 123851, Sep. 2021, doi: 10.1016/J.CONBUILDMAT.2021.123851.

[26] G. Heydari, E. Thormann, M. Järn, E. Tyrode, and P. M. Claesson, "Hydrophobic surfaces: Topography effects on wetting by supercooled water and freezing delay," *J. Phys. Chem. C*, vol. 117, no. 42, pp. 21752–21762, Oct. 2013, doi: 10.1021/JP404396M.

[27] Y. Li, D. R. Dekel, and O. Manor, "Surface Acoustic Wave Mitigation of Precipitate Deposition on a Solid Surface─An Active Self-Cleaning Strategy," *ACS Appl. Mater. Interfaces*, vol. 13, no. 49, pp. 59471–59477, Dec. 2021, doi: 10.1021/ACSAMI.1C17778/SUPPL_FILE/AM1C17778_SI_001.PDF.

[28] S. Milles, M. Soldera, B. Voisiat, and A. F. Lasagni, "Fabrication of superhydrophobic

and ice-repellent surfaces on pure aluminium using single and multiscaled periodic textures," *Sci. Reports 2019 91*, vol. 9, no. 1, pp. 1–13, Sep. 2019, doi: 10.1038/s41598-019-49615-x.

[29] Y. Zhuo, V. Håkonsen, Z. He, S. Xiao, J. He, and Z. Zhang, "Enhancing the Mechanical Durability of Icephobic Surfaces by Introducing Autonomous Self-Healing Function," *ACS Appl. Mater. Interfaces*, vol. 10, no. 14, pp. 11972–11978, Apr. 2018, doi: 10.1021/ACSAMI.8B01866.

[30] K. K. Varanasi, T. Deng, J. D. Smith, M. Hsu, and N. Bhate, "Frost formation and ice adhesion on superhydrophobic surfaces," *Appl. Phys. Lett.*, vol. 97, no. 23, p. 234102, Dec. 2010, doi: 10.1063/1.3524513.

[31] X. Tan *et al.*, "Employing micro pyramidal holes and porous nanostructures for enhancing the durability of lubricant-infused surfaces in anti-icing," *Surf. Coatings Technol.*, vol. 405, p. 126568, Jan. 2021, doi: 10.1016/J.SURFCOAT.2020.126568.

[32] J. Li, E. Ueda, D. Paulssen, and P. A. Levkin, "Slippery Lubricant-Infused Surfaces: Properties and Emerging Applications," *Adv. Funct. Mater.*, vol. 29, no. 4, p. 1802317, Jan. 2019, doi: 10.1002/ADFM.201802317.

[33] H. Niemelä-Anttonen *et al.*, "Icephobicity of Slippery Liquid Infused Porous Surfaces under Multiple Freeze–Thaw and Ice Accretion–Detachment Cycles," *Adv. Mater. Interfaces*, vol. 5, no. 20, Oct. 2018, doi: 10.1002/ADMI.201800828.

[34] H. He and Z. Guo, "Superhydrophobic materials used for anti-icing Theory, application, and development," *iScience*, vol. 24, no. 11, p. 103357, Nov. 2021, doi: 10.1016/J.ISCI.2021.103357.

[35] H. Fallahi, J. Zhang, H. P. Phan, and N. T. Nguyen, "Flexible Microfluidics: Fundamentals, Recent Developments, and Applications," *Micromachines*, vol. 10, no. 12, Dec. 2019, doi: 10.3390/MI10120830.

[36] Y. Q. Fu *et al.*, "Advances in piezoelectric thin films for acoustic biosensors, acoustofluidics and lab-on-chip applications," *Prog. Mater. Sci.*, vol. 89, pp. 31–91, Aug. 2017, doi: 10.1016/J.PMATSCI.2017.04.006.

[37] D. Yang *et al.*, "Nanoscale 'Earthquake' Effect Induced by Thin Film Surface Acoustic Waves as a New Strategy for Ice Protection," *Adv. Mater. Interfaces*, vol. 8, no. 2, p. 2001776, Jan. 2021, doi: 10.1002/admi.202001776.

[38] V. Daniliuk, Y. Xu, R. Liu, T. He, and X. Wang, "Ultrasonic de-icing of wind turbine blades: Performance comparison of perspective transducers," *Renew. Energy*, vol. 145, pp. 2005–2018, Jan. 2020, doi: 10.1016/J.RENENE.2019.07.102.

[39] S. Damiati, U. B. Kompella, S. A. Damiati, and R. Kodzius, "Microfluidic Devices for Drug Delivery Systems and Drug Screening," *Genes (Basel).*, vol. 9, no. 2, Feb. 2018, doi: 10.3390/GENES9020103.

[40] M. Stringer *et al.*, "Methodologies, technologies, and strategies for acoustic streaming-based acoustofluidics," *Appl. Phys. Rev.*, vol. 10, no. 1, p. 011315, Mar. 2023, doi: 10.1063/5.0134646.

[41] Y. Wang *et al.*, "Flexible/Bendable Acoustofluidics Based on Thin-Film Surface Acoustic Waves on Thin Aluminum Sheets," *ACS Appl. Mater. Interfaces*, vol. 13, no. 14, pp. 16978–16986, Apr. 2021, doi:

10.1021/ACSAMI.0C22576/SUPPL_FILE/AM0C22576_SI_008.AVI.

[42] Y. Gao, Y. Li, and X. Ding, “Acoustofluidic technology for cell biophysics,” *Micro Nano Syst. Biophys. Stud. Cells Small Org.*, pp. 153–171, Jan. 2021, doi: 10.1016/B978-0-12-823990-2.00007-6.

[43] K. Uchino, “Piezoelectric ceramics for transducers,” *Ultrason. Transducers Mater. Des. Sensors, Actuators Med. Appl.*, pp. 70–116, Jan. 2012, doi: 10.1533/9780857096302.1.70.

[44] G. Potter, N. Tokranova, A. Rastegar, and J. Castracane, “Design, fabrication, and testing of surface acoustic wave devices for semiconductor cleaning applications,” *Microelectron. Eng.*, vol. 162, pp. 100–104, Aug. 2016, doi: 10.1016/J.MEE.2016.04.006.

[45] Z. Wang, “Recent progress on ultrasonic de-icing technique used for wind power generation, high-voltage transmission line and aircraft,” *Energy Build.*, vol. 140, pp. 42–49, Apr. 2017, doi: 10.1016/J.ENBUILD.2017.01.072.

[46] D. Yang *et al.*, “Dynamic Mitigation Mechanisms of Rime Icing with Propagating Surface Acoustic Waves,” *Langmuir*, 2022, doi: 10.1021/ACS.LANGMUIR.2C01509.

[47] J. Zhou *et al.*, “Transparent surface acoustic wave devices on Zno/Glass using Al-doped Zno as the electrode,” *IEEE Electron Device Lett.*, vol. 34, no. 10, pp. 1319–1321, 2013, doi: 10.1109/LED.2013.2276618.

[48] M. Kadota and C. Kondoh, “Influence of step-like portions on the surface of zno/glass saw filters on their frequency characteristics,” *IEEE Trans. Ultrason. Ferroelectr. Freq. Control*, vol. 44, no. 3, pp. 658–665, 1997, doi: 10.1109/58.658325.

[49] J. Zhou *et al.*, “Transparent ZNO/glass surface acoustic wave devices with aluminum doped ZNO electrode,” *Proc. IEEE Int. Conf. Micro Electro Mech. Syst.*, pp. 691–695, Feb. 2017, doi: 10.1109/MEMSYS.2017.7863502.

[50] W. B. Wang *et al.*, “Transparent ZnO/glass surface acoustic wave based high performance ultraviolet light sensors,” *Chinese Phys. B*, vol. 24, no. 5, p. 057701, 2015, doi: 10.1088/1674-1056/24/5/057701.

[51] H. Song, D. Jang, J. Lee, K. Yong Lee, and S. Kug Chung, “SAW-driven self-cleaning drop free glass for automotive sensors,” *J. Micromechanics Microengineering*, vol. 31, no. 12, p. 125007, Oct. 2021, doi: 10.1088/1361-6439/AC2FEC.

[52] H. Kim, R. O. Bonsu, C. Odonohue, R. Y. Korotkov, L. McElwee-White, and T. J. Anderson, “Aerosol-assisted chemical vapor deposition of tungsten oxide films and nanorods from oxo tungsten(VI) fluoroalkoxide precursors,” *ACS Appl. Mater. Interfaces*, vol. 7, no. 4, pp. 2660–2667, Feb. 2015, doi: 10.1021/AM507706E.

[53] H. Zhang and H. Wang, “Investigation of Surface Acoustic Wave Propagation Characteristics in New Multilayer Structure: SiO2/IDT/LiNbO3/Diamond/Si,” *Micromachines 2021, Vol. 12, Page 1286*, vol. 12, no. 11, p. 1286, Oct. 2021, doi: 10.3390/MI12111286.

[54] L. Haworth *et al.*, “Reduction of ice adhesion on nanostructured and nanoscale slippery surfaces,” *Nanotechnol. Precis. Eng.*, vol. 6, no. 1, p. 013007, Feb. 2023, doi: 10.1063/10.0017254.

[55] H. F. Pang *et al.*, “Characterization of the surface acoustic wave devices based on ZnO/nanocrystalline diamond structures,” *Phys. status solidi*, vol. 210, no. 8, pp. 1575–1583, Aug. 2013, doi: 10.1002/PSSA.201228631.

[56] H. Ong *et al.*, “ZnO/glass thin film surface acoustic waves for efficient digital acoustofluidics and active surface cleaning,” *Mater. Chem. Phys.*, vol. 287, p. 126290, Aug. 2022, doi: 10.1016/J.MATCHEMPHYS.2022.126290.

[57] D. Yang *et al.*, “Dynamic mitigation mechanisms of rime icing with propagating surface acoustic waves - Northumbria Research Link,” *Langmuir*, no. 0743, p. 7463, 2022, [Online]. Available: https://doi.org/10.1021/acs.langmuir.2c01509.

[58] Y. Yoshino, M. Takeuchi, K. Inoue, T. Makino, S. Arai, and T. Hata, “Control of temperature coefficient of frequency in zinc oxide thin film bulk acoustic wave resonators at various frequency ranges,” *Vacuum*, vol. 66, no. 3–4, pp. 467–472, Aug. 2002, doi: 10.1016/S0042-207X(02)00117-3.

[59] D. N. Sibley, P. Llombart, E. G. Noya, A. J. Archer, and L. G. MacDowell, “How ice grows from premelting films and water droplets,” *Nat. Commun.*, vol. 12, no. 1, 2021, doi: 10.1038/s41467-020-20318-6.

[60] J. H. Snoeijer and P. Brunet, “Pointy ice-drops: How water freezes into a singular shape,” *Am. J. Phys.*, vol. 80, no. 9, pp. 764–771, 2012, doi: 10.1119/1.4726201.

[61] M. Alghane, Y. Q. Fu, B. X. Chen, Y. Li, M. P. Y. Desmulliez, and A. J. Walton, “Frequency effect on streaming phenomenon induced by Rayleigh surface acoustic wave in microdroplets,” *J. Appl. Phys.*, vol. 112, no. 8, p. 084902, Oct. 2012, doi: 10.1063/1.4758282.

[62] M. B. Dentry, L. Y. Yeo, and J. R. Friend, “Frequency effects on the scale and behavior of acoustic streaming,” *Phys. Rev. E - Stat. Nonlinear, Soft Matter Phys.*, vol. 89, no. 1, Jan. 2014, doi: 10.1103/PHYSREVE.89.013203.